Quantum Limited Optical Phase Detection in a High Power Suspended Interferometer

by

Brian Thomas Lantz

Submitted to the Department of Physics in partial fulfillment of the requirements for the degree of

Doctor of Philosophy

at the

MASSACHUSETTS INSTITUTE OF TECHNOLOGY

February, 1999

Author .....

Department of Physics
February, 1999

Certified by .....

Rainer Weiss
Department of Physics
Thesis Supervisor

Accepted by .....

Thomas J. Greytak
Professor, Associate Department Head for Education
Department of Physics

LIGO-P990003-00-R

Quantum Limited Optical Phase Detection in a High Power Suspended Interferometer

by

Brian Lantz

Submitted to the Department of Physics in February 1999,
in partial fulfillment of the requirements for the degree of
Doctor of Philosophy

Abstract

The LIGO project (Laser Interferometer Gravitational-Wave Observatory) is currently engaged in the construction of a new observatory to measure gravitational radiation from astrophysical sources. The first generation of interferometric gravitational wave antennas is scheduled to come on-line in 2001. With an initial noise level of 3×10^{-23} strain$/\sqrt{\text{Hz}}$ at frequencies around 200Hz, these antennas represent the most sensitive instruments ever constructed for the detection of gravitational radiation. To achieve the required sensitivity, the antennas are configured as recycled Michelson Interferometers with Fabry-Perot cavities in the Michelson arms.

One of the fundamental limits associated with an instrument of this type is the ability to detect differential phase shifts between the beams returning to the beamsplitter from the Fabry-Perot arm cavities. To achieve the planned sensitivity to gravitational radiation, this detection should be limited only by photon counting statistics ("shot noise") at a level of 8×10^{-11} radians$/\sqrt{\text{Hz}}$ between 150Hz and 10kHz.

The goal of this work is to develop and demonstrate the techniques which are necessary to achieve this optical phase sensitivity. A prototype recycled Michelson interferometer was constructed which reached an optical phase sensitivity of 12×10^{-11} radians$/\sqrt{\text{Hz}}$ above 600 Hz.

This thesis describes the methods used to achieve this optical phase sensitivity, and details the lessons learned from operating the prototype instrument. We pay particular attention to interferometric control of suspended optics, laser frequency control, and thermal lensing.

Thesis Supervisor: Rainer Weiss
Title: Professor of Physics

Acknowledgments

To Rai, who talked with me one Saturday morning and set me off in a new direction.

To Peter Fritschel, whose quiet brilliance made this experiment possible.

To Gaby, who must be the best lab partner one could hope for.

To Partha and Haisheng, who worked tirelessly to make this project a success.

To Nergis and Daniel, for a damn fine wavefront sensor which worked on the first day!

To Jim, Rich, and Rick, who gave us the Prestabilized Laser. Either it ran like a champ, or Rich would fly to Boston and fix it.

To the LIGO team, for the technical support, guidance, and friendship which made this experiment a success. You will change the world, good luck!

To Jen, the love of my life and the light of my heart, my constant companion, even when I was writing my thesis.

"In the first experiment one of the principal difficulties encountered . . . was its extreme sensitiveness to vibration. This was so great that it was impossible to see the interference fringes except at brief intervals when working in the city, even at two o'clock in the morning."

-Albert Michelson, [Michelson 1887]

(Describing the first interferometer he used to attempt to detect the luminiferous ether.)

Table of Contents

List of Figures

Chapter 1

Importance of Optical Phase Sensitivity to Interferometric Gravitational Wave Antennas

1.1 Introduction

The Laser Interferometer Gravitational-Wave Observatory (LIGO) is now engaged in construction of a new observatory which will be able to measure gravitational radiation from astrophysical sources [Abramovici '92]. Gravitational radiation was first predicted by Einstein [Einstein '16], [Einstein '18], but, due to the extremely small influence of this radiation, it has never been directly observed.[1] The goal of this chapter is to introduce the reader to effects of gravitational radiation, explain briefly the method which LIGO will use to detect this radiation, and motivate this work by describing the importance of optical phase sensitivity to the LIGO detection scheme.

1.2 Gravitational Waves

Gravitational waves are traveling waves of the space-time metric, $g_{\mu\upsilon}$. Generated by accelerating masses, these gravitational field disturbances propagate at the speed of light, and provide the solution to Newton's problem of gravitational action at a distance. A gravitational plane wave creates a differential strain along the 2 space axes which are transverse to the direction of the waves's propagation. For any reasonable source of gravitational radiation, the perturbations of the metric by the passing gravitational wave are quite small, so we use the "linearized" theory (see, for example, [Schutz '90] or [Saulson '94]) and rewrite the metric $g_{\mu\upsilon}$ as

$$g_{\mu\upsilon} \approx \eta_{\mu\upsilon} + h_{\mu\upsilon}, \quad |h_{\mu\upsilon}| \ll 1 \tag{1.1}$$

where $\eta_{\mu\upsilon}$ is the Minkowski metric (describing flat space), and $h_{\mu\upsilon}$ is the metric distortion due to the gravitational wave. In the weak-field limit, the Einstein equation for $h_{\mu\upsilon}$ can be written as a traveling wave equation,

1. However, indirect observations have been made by Hulse & Taylor [Hulse '75], [Taylor '82], [Taylor '89], who carefully studied the orbital decay of a neutron star binary system, and found the decay rate to be in excellent agreement with the energy lost to gravitational radiation.

$$\left(-\frac{1}{c^2}\frac{\partial^2}{\partial t^2} + \nabla^2\right) h_{\mu\upsilon} = 0. \tag{1.2}$$

In a transverse-traceless gauge, we can write the solution for a wave traveling in the $\hat{z}$ direction as

$$h_{\mu\upsilon} = \exp(ik_\alpha x^\alpha) \begin{bmatrix} 0 & 0 & 0 & 0 \\ 0 & h_+ & h_x & 0 \\ 0 & h_x & -h_+ & 0 \\ 0 & 0 & 0 & 0 \end{bmatrix}. \tag{1.3}$$

This represents two independent plane-wave solutions. The magnitude of the spatial components along h_{xx} and h_{yy} is h_+, which is known as the "plus" polarization, and the magnitude along h_{xy} and h_{yx} is h_x, which is commonly called the "cross" polarization. Eqn. 1.3 means that each of the four non-zero components of $h_{\mu\upsilon}$ could be expressed as

$$h_{xx} = h_+ \cdot \sin(-\omega t + kz) \tag{1.4}$$

representing a metric perturbation traveling along $\hat{z}$ at the speed of light, with frequency ω, and amplitude h_+.

One way to understand the implication of a passing gravitational wave is to examine the change in proper distance between two objects as a wave passes by. With one object at the origin, and the second at $x = l$, $y = z = 0$, then the proper distance between them is

$$D_{\text{proper}} = \int \left| g_{\mu\upsilon} dx^\mu dx^\upsilon \right|^{\frac{1}{2}}. \tag{1.5}$$

This reduces to

$$D_{\text{proper}} = \int_0^l \sqrt{|g_{xx}|}\, dx \tag{1.6}$$

If h_+ is spatially uniform, changing slowly[2], and less than 1, then the proper distance is:

$$\begin{aligned} D_{\text{proper}} &\approx l \cdot \sqrt{\eta_{xx} + h_{xx}(x = 0, t = 0)} \\ &\approx l \cdot \left[1 + \frac{1}{2} h_+(x = 0, t = 0)\right] \end{aligned} \tag{1.7}$$

2. The measurement in LIGO will be conducted by light which is resonant in a 4km arm cavity, so the time fluctuations of $h_{\mu\nu}$ should be compared with the cavity storage time of 0.88 msec.

which means the distance between the two "freely-falling" objects changes as a gravitational wave passes by. According to eqn. 1.3, $h_{xx} = -h_{yy}$, so as distances along the $\hat{x}$ axis are elongated, distances along $\hat{y}$ will be compressed by the same ratio. It is important to realize that the proper distance is stretched by an amount which is proportional to the original distance and the gravitational wave amplitude, which is why the effect of gravitational radiation is usually described as producing a strain, i.e.

$$\frac{\delta l}{l} = \frac{1}{2}h_{+} \tag{1.8}$$

There are only two independent components of $h_{\mu\upsilon}$, which are described as the two polarizations of gravitational waves. The amplitude of a plane wave in the "plus" polarization is captured by h_{+}, which will differentially change the proper distances along $\hat{x}$ and $\hat{y}$. The "cross" polarization is described by h_{x}, and results in a differential stretching which is rotated by 45° from the $\hat{x}$ and $\hat{y}$ axes. This effect on a ring of free masses is shown in figure 1.1.

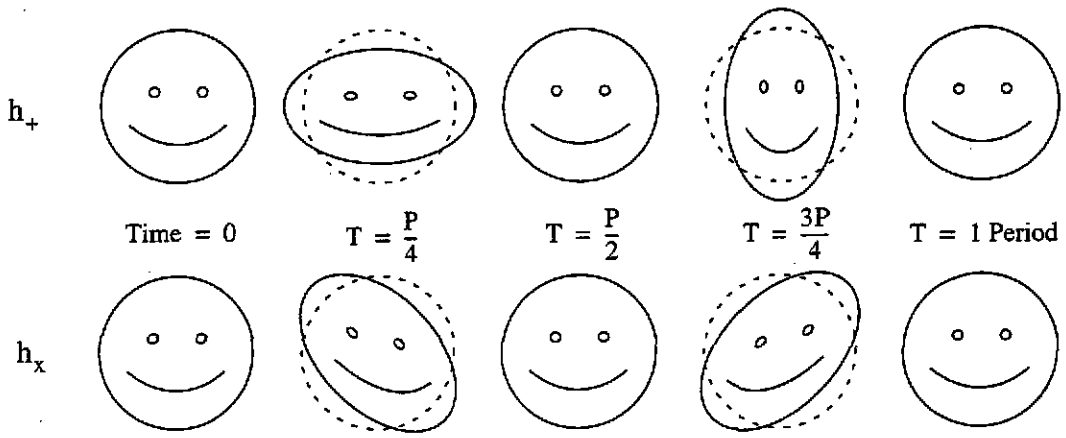

Figure 1.1: The effect of a passing gravitational wave on an object.

1.3 Sources of Gravitational Waves

The search for gravitational waves has so far been stymied by the fact that even the most powerful sources of gravitational radiation only produce tiny effects at the Earth. A typical source produces waves at the earth with a strain of $h \sim \ddot{Q}G/Rc^4$. Here, $\ddot{Q}$ is the acceleration of the quadrupole moment of the source, G is the gravitational constant, R is the distance from the source, and c is the speed of light. The scaling factor, G/c^4, is quite small, leading us to consider gravitational radiators on the order of a solar mass.

Many sources of gravitational waves are discussed as possible LIGO candidates, including coalescence of two compact objects (such as neutron stars or black holes), supernovas which generate non-spherical motion during the core collapse, and spinning neutron stars with non-axisymmetric mass distribution (see, for example, [Thorne '87]). The imminent completion of the LIGO interferometers and data from the new Rossi X-Ray Timing Explorer (RXTE) have generated a great deal of interest in variants to these standard sources, including new estimates of the number of neutron star-black hole binaries by Bethe and Brown [Bethe '98] and work by Lars Bildsten and others discussing various mechanisms by which neutron stars could convert the energy and angular momentum gained by accretion into gravitational radiation [Andersson '98], [Bildsten '98], [Owen '98].

The fiducial source of radiation for which one designs detectors is the burst of gravitational waves produced in the final minutes before the coalescence of inspiralling binary neutron stars. If two neutron stars of equal mass M are orbiting in the x-y plane at a distance $2r_0$ from each other with an orbital frequency of $f_{\rm orb}$, then the amplitude of waves traveling along the $\hat{z}$ axis is [Saulson '94]

$$\begin{aligned} h_{xx} &= \frac{32\pi^2 G}{Rc^4} M r_0^2 f_{\rm orb}^2 \cos(2 \cdot 2\pi f_{\rm orb} t), \\ h_{xy} &= -h_{xx}. \end{aligned} \tag{1.9}$$

Newtonian mechanics suggests we can relate the radius and frequency by $f_{\rm orb}^2 = GM/16\pi^2 r_0^3$, and the strain becomes

$$h_{xx} = \frac{2G^2M^2}{Rc^4 r_0} = 1.1\times10^{-21}\left(\frac{M}{1.4M_\odot}\right)^{\frac{2}{3}}\left(\frac{15\ \text{Mpc}}{R}\right)\left(\frac{f_{\rm orb}}{400\ \text{Hz}}\right)^{\frac{2}{3}}. \tag{1.10}$$

This represents the strain produced by a pair of neutron stars ($M = 1.4M_\odot$) in the Virgo cluster ($R = 15$ Mpc) in the last minute of their lives (when $f_{\rm orb} \sim 400$Hz!). It is this level of strain which LIGO hopes to detect. Unfortunately, current estimates of the population of neutron star binaries indicate that we will need to observe an astrophysical volume which extends 200 Mpc from Earth to measure three such coalescence events each year ([Phinney '91] and [Narayan '91]).

Another burst source is the core collapse of a type II supernova. Several models of core collapse are described in [Thorne '87]. The current belief is that the core collapse will be only slightly aspheric. If bar (m=2) modes form in the spinning, collapsing core, they would emit gravitational radiation. These events might last about 30 cycles at 1000Hz, and could emit gravitational energy $\Delta E_{GW} \sim 3\times10^{-4} M_{\odot} c^2$. At a distance of 10Mpc, within which volume there are typically several type II supernovas each year, a core collapse which develops a bar instability could generate a characteristic strain at the Earth of $h_c \sim 5\times10^{-22}$.

There are several models for periodic sources, sources whose gravitational radiation signature changes very slowly with time. Many of these sources, like the Hulse-Taylor binary pair of neutron stars PSR1916+13, emit radiation at a frequency much to low to be seen with currently imagined Earth-bound instruments[3]. Some periodic sources have been suggested, however, which would be within the observational capabilities of the LIGO detectors. [Bildsten '98] has suggested, for example, that the accreting neutron star in Scorpius X-1 could be emitting gravitational waves at 500Hz, twice the neutron star rotation frequency. The amplitude could be as large as $h_c \approx 2.2\times10^{-26}$, which means it should be observable with a year or so of integrated observation time.

1.4 The LIGO detector

To detect a strain of the order 10^{-21} will be difficult, but several groups around the world are currently building observatories to meet that challenge. LIGO is building a pair of 4km baseline optical interferometers, one in Hanford, Washington, and one in Livingston Parish, Louisiana [Barish '97]. LIGO is also building a half length (2 km) interferometer in the vacuum system at the Hanford site. Virgo, an Italian-French collaboration, is building a 3km instrument near Pisa, Italy [Vinet '97]. GEO600 is a German-U.K. collaboration building an advanced 600 meter instrument in Hanover, Germany [Danzmann '97]. There is also active work ongoing at the TAMA project in Japan [Tsubono '97] and the ACIGA project in Australia [Blair '97].

Each of the LIGO instruments is configured as a power-recycled Michelson interferometer with Fabry-Perot arm cavities, as shown in figure 1.2. The Michelson interferome-

3. However, LISA, the proposed Laser Interferometer Space Antenna, could readily observe many low frequency sources within our galaxy [Folkner '98].

ter is well suited for the detection of gravitational waves, because it is sensitive to differential arm length changes.

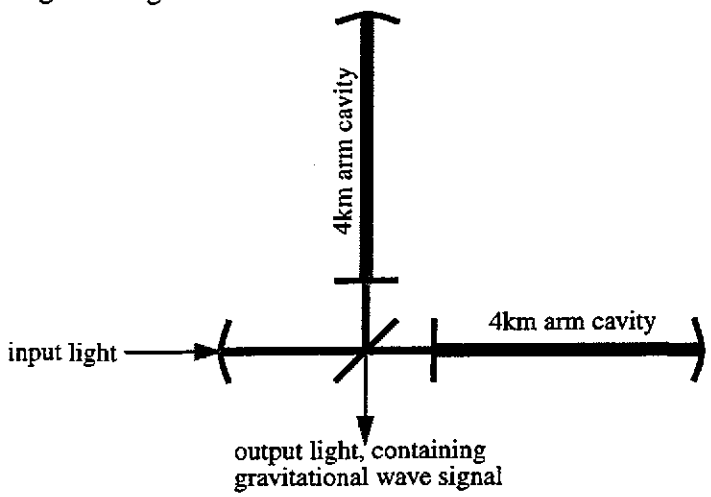

Figure 1.2: Basic optical configuration of LIGO.
This figure shows the recycling mirror, the beamsplitter, and the Fabry-Perot arm cavities. The line thickness indicates that there is more power circulating in the arm cavities than is circulating at the beamsplitter, and that there is more power at the beamsplitter than in the input beam.

If the mirrors are configured as free masses[4] and the wave is incident on the interferometer from the correct direction, then the perpendicular arms will experience a differential strain as the space is distorted as shown in figure 1.1. In the direction of maximum sensitivity, for a wave polarized in the "plus" direction, one arm will see a strain of $+\frac{1}{2}h_+$ and the other arm will see a strain of $-\frac{1}{2}h_+$, so the differential strain $h = h_+$. As the wave passes through the interferometer, alternately expanding and compressing the arms, the differential phase shift of the two beams returning to the beamsplitter from the arms will oscillate at the gravitational wave frequency.

In effect, the interferometer arms are a transducer which converts gravitational wave strain into differential optical phase shifts. Since the waves are of low amplitude, the LIGO transducer must be extremely sensitive. The challenges to building a good detector fall into three broad areas:

1. Build a transducer which effectively converts gravitational wave strain into optical phase shift.

2. Make the differential optical phase insensitive to other sources of noise.

3. Make a very sensitive detection of the resulting differential optical phase.

4. The LIGO masses are suspended as pendula with a 1Hz fundamental frequency, which means they are essentially free in the measurement band, which ranges from 100Hz to 10kHz.

To meet the first challenge and make the LIGO interferometer more sensitive to gravitational waves, Fabry-Perot optical storage cavities are built into each arm of the LIGO detector, so the light effectively bounces back and forth in the arm many times before returning to the beamsplitter. By making the light beam traverse the arm length multiple times, the light accumulates extra phase shift. One can increase the optical phase shift for a given gravitational wave by increasing the arm cavity storage time, up to the point where the storage time is half the gravitational wave period, at which point further storage time offers no advantages.

The conversion of gravitational wave strain into differential phase shift is given by

$$\left|\frac{\delta\phi}{\delta h}\right| = \frac{8\pi\nu_l\tau_s}{\sqrt{1+(4\pi f\tau_s)^2}} = \frac{6.2\times10^{12}}{\sqrt{1+\left(\frac{f}{90\text{Hz}}\right)^2}} \text{ radians of phase shift per unit strain} \quad (1.11)$$

where ϕ is the optical phase shift, h is the gravitational wave amplitude, f is the gravitational wave frequency, $\nu_l = 2.8\times10^{14}$Hz is the laser frequency (the laser wavelength is 1.064 μm), and $\tau_s = 8.8\times10^{-4}$sec. is the optical storage time of the arm cavity.

The second challenge is to be insensitive to other effects which might cause differential phase shifts, such as seismic motion and thermal motion which can drive the mirrors and change the arm length. This is why the arm cavities are each 4km long. As the arm length increases, one can maintain the optical storage time while decreasing the number of times the light bounces off of each end mirror, thereby reducing optical losses and minimizing sensitivity to motions of the optics caused by thermal noise and seismic noise.

The third challenge is to be as sensitive as possible to differential phase shifts at the beamsplitter. Even though the LIGO interferometers should be excellent transducers, a strain of 10^{-21} only results in a differential phase shift of 4×10^{-9} radians.

The optical phase sensitivity requirements for LIGO can be deduced from the target noise floor shown in figure 1.3 (from the LIGO Science Requirements Document [LIGO SRD '95]). Below 150Hz the noise floor is caused by random mirror motion which is driven by seismic and thermal noise. Above 150Hz, the noise floor is limited by the optical phase sensing limit set by photon counting statistics, colloquially known as "shot noise." This limit is determined from the gravitational strain to optical phase conversion efficiency

for LIGO (given by eqn. 1.11) times a shot noise limited optical phase sensitivity of $7\times10^{-11}\text{radians}/\sqrt{\text{Hz}}$.

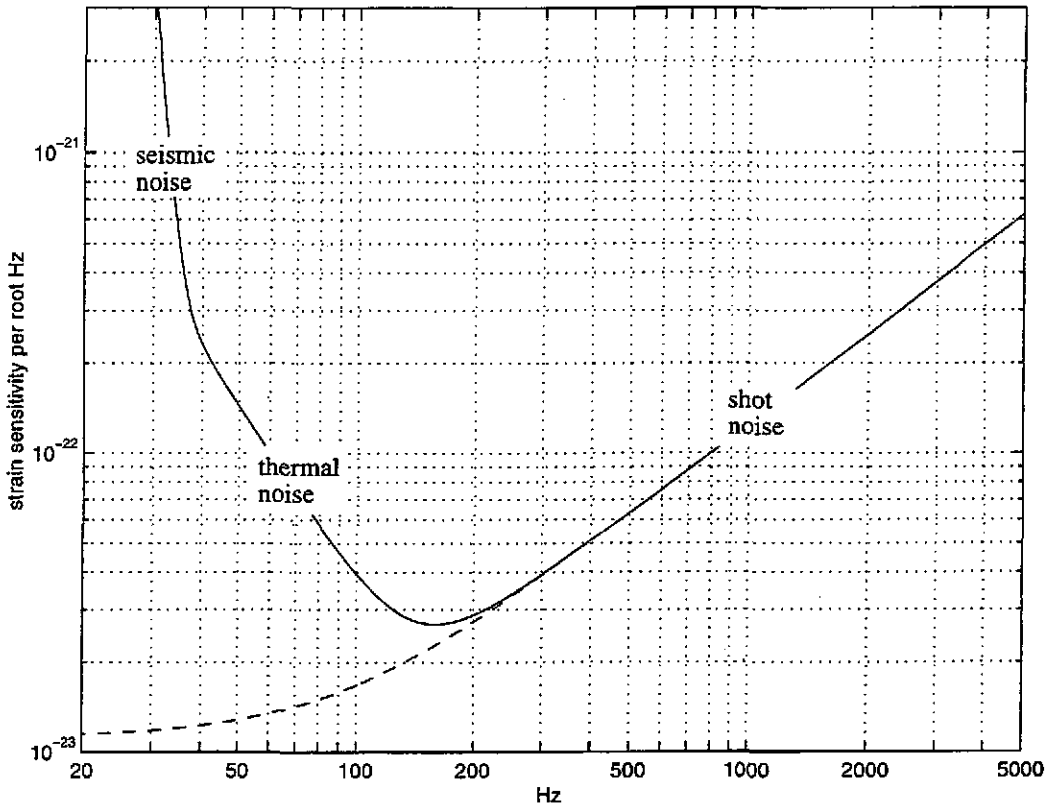

Figure 1.3: LIGO noise curve. The solid line is the total noise floor, and the dashed line is the shot noise limit contribution to that noise.

This level of phase sensitivity has never been demonstrated for this type of instrument. The detection of these small phase *differences* is the focus of this thesis.

In chapter 2, we show the basic optical configuration and readout scheme for our experiment, and describe the fundamental phase sensitivity for this type of interferometer. The ultimate limit of sensitivity is set by the statistics of photon arrival. We show that as the photon arrival rate increases, the signal to noise ratio improves as $1/\sqrt{\text{Optical power}}$.

The Phase Noise Interferometer (PNI) is described in chapter 3, along with the steps taken to control the instrument and reduce the noise at the output. The results of the experiment are described in chapters 4 and 5. Chapter 4 discusses one of the most serious problems we encountered, thermal lensing, and chapter 5 describes the final spectrum measured with the instrument.

Chapter 2

Interferometer Configuration and Sensitivity Limits

One fundamental limit of the fringe sensitivity of a Michelson interferometer is determined by the statistics of photon counting. In this chapter we develop the theoretical sensitivity limit for the frontally-modulated power-recycled Michelson interferometer used in this experiment. The basic layout of the interferometer we use is shown below in figure 2.1. We first develop the sensitivity of a simple Michelson interferometer, describe the Schnupp modulation scheme we use to measure the changes in the Michelson interferometer arm length, and discuss the impact of adding power recycling. We then calculate the maximum signal to noise ratio such an interferometer can achieve based on a quantum mechanical description of the photon arrival statistics.

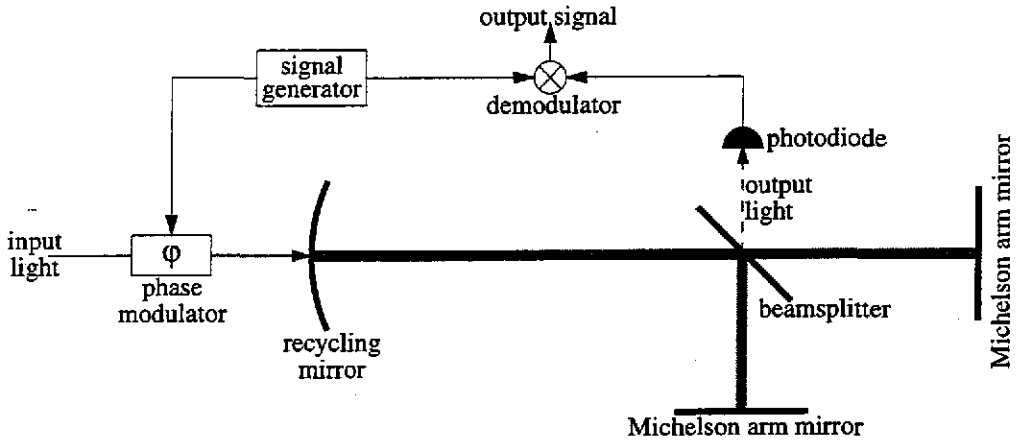

Figure 2.1: Schematic view of recycled Michelson interferometer with frontal modulation
The modulator puts phase modulation sidebands onto the light, the sidebands are used by the readout scheme to determine how far the Michelson interferometer (the three mirrors on the right side of the diagram) is from the optimal working point. The two arms of the Michelson interferometer have macroscopically different lengths, which is required by the readout scheme.

2.1 Michelson Interferometer Sensitivity and Schnupp Modulation

Description

A simple Michelson interferometer comprises a beamsplitter and two arm mirrors. The beamsplitter divides an incident laser beam into two output beams, which are reflected by the arm mirrors back to the beamsplitter where they interfere. The interference between the two return beams gives information about the relative length of the arms. Figure 2.2 shows the beams for this configuration.

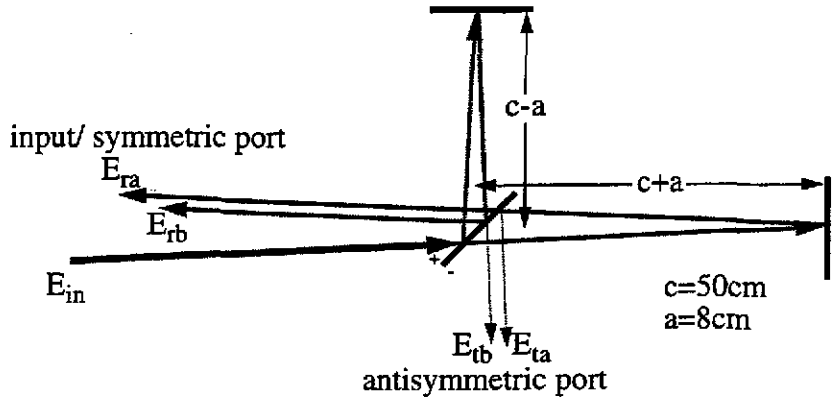

Figure 2.2: Schematic view of an asymmetric Michelson interferometer.
The incident and reflected beams in the PNI are coaxial, but have been separated in this diagram for clarity. Although the symbol placement implies some propagation distance, the fields E_{in}, E_t, and E_r are defined immediately after their last beamsplitter interaction.

The Michelson interferometer arms in this experiment were different lengths. A macroscopic asymmetry adds a frequency selectivity to the transfer function, and is a key part of the length measurement scheme. The length (and angle, see section 3.4) detection is accomplished with a RF heterodyne technique called Schnupp Modulation. [Schnupp '86, see also Regehr '95.] Phase modulation sidebands are impressed on the light before it enters the interferometer (hence the term frontal modulation), and differential misalignments convert the phase modulation into amplitude modulation at the antisymmetric port of the beamsplitter. The Michelson interferometer's antisymmetric port is held at a dark fringe, so ideally none of the power of the carrier is transmitted to the detector, instead, it is reflected back towards the laser. However, the concept behind Schnupp modulation is that the macroscopic asymmetry forces some of the power in the sidebands to be transmitted through the antisymmetric port. If the carrier begins to slip away from the dark fringe, carrier light transmitted out of the dark port begins to beat against sidebands, producing the RF amplitude modulation which we measure.

This scheme was chosen for the LIGO readout because it enables power recycling (discussed in the next section), allows frontal modulation (so the modulators do not experience the full recycled light power), and requires a minimum number of large, suspended optics (which are complicated and expensive). To meet LIGO's requirements, there will be 300 Watts of power incident on the LIGO beamsplitter [LIGO SRD '95]. By using a fron-

tally-modulated, recycled configuration, LIGO can reach high circulating power levels with only 10 Watts of input power, no active intracavity optical elements, and only a few watts of output power on the photodetectors.

Michelson Interferometer's Response to Phase Modulated Light

A recycled Michelson interferometer can be described as a series of simpler optical elements. One element is the unrecycled asymmetric Michelson interferometer. Following figure 2.2, we describe the electric fields of the four exit paths [following Gonzalez '97]:

$$E_{ra}(k) = E_{in} \cdot t_{BS}^2 \cdot e^{-ik2(c+a)}$$

$$E_{rb}(k) = E_{in} \cdot r_{BS}^2 \cdot e^{-ik2(c-a)}$$

$$E_{ta}(k) = E_{in} \cdot t_{BS} \cdot -r_{BS} \cdot e^{-ik2(c+a)}$$

$$E_{tb}(k) = E_{in} \cdot t_{BS} \cdot r_{BS} \cdot e^{-ik2(c-a)}.$$

Here, r_{BS} and t_{BS} are the field reflectivity and transmission, respectively, of the beamsplitter, k is the wavenumber of light, c is the average, one-way length of the arms (50cm) and a is the asymmetry (8cm). The reflected fields are coaxial, as are the transmitted fields; the total field of the reflected beam is

$$E_r(k) = E_{ra}(k) + E_{rb}(k) = E_{in}[t_{BS}^2 \cdot e^{-ik2(c+a)} + r_{BS}^2 \cdot e^{-ik2(c-a)}]. \quad (2.1)$$

We can rewrite the field in terms of the fractional power the beamsplitter transmits and reflects, and the difference between them.

$$T_{BS} \equiv t_{BS}^2, \; R_{BS} \equiv r_{BS}^2, \; U_{BS} \equiv R_{BS} - T_{BS}$$

The reflected field then becomes

$$\begin{aligned} E_r(k) &= E_{in}\, e^{-ik2c}(\cos(2ka) + iU_{BS}\sin(2ka)) \\ &\approx E_{in}\, e^{-ik2c}\cos(2ka) \end{aligned} \quad (2.2)$$

for a 50/50 beamsplitter. The field transmitted to the other port of the Michelson interferometer (alternately called the antisymmetric port or the dark port) takes the form

$$E_t(k) = E_{ta}(k) + E_{tb}(k) = 2iE_{in} \cdot t_{BS} \cdot r_{BS} \cdot e^{-ik2c} \cdot \sin(2ka). \quad (2.3)$$

If the beamsplitter is not perfectly balanced, then the minimum reflected field increases from 0 to $E_r(k)_{min} = E_{in}\, U_{BS}$, but the maximum reflected field remains the same (which

is where this experiment operates). The biggest effect an unequal beamsplitter would have is to reduce the transmitted light. The reduction factor is $\sqrt{1-U_{BS}^2} \approx 1-0.01$ for our beamsplitter (see chapter 5), so this effect has been ignored. Equations 2.2 and 2.3 are true for any wavenumber, k. We can specialize these expressions to describe the salient features of the Michelson interferometer in this experiment.

The first specialization involves the laser light incident on the interferometer. The light from the laser is single frequency and single spatial mode. The light is passed through a resonant phase modulator which adds sidebands to the light which are separated from the carrier frequency by ω_m radians/sec. The light at the output of the phase modulator has the form

$$\begin{aligned}\overrightarrow{E_{in}}(t) &= E_{in}e^{i\{\omega t+\Gamma\sin(\omega_m t)\}} \\ &\approx E_{in}e^{i\omega t}[J_0(\Gamma)+2iJ_1(\Gamma)\sin(\omega_m t)+O(J_2(\Gamma))] \\ &\approx E_{in}e^{i\omega t}[J_0(\Gamma)+J_1(\Gamma)e^{i\omega_m t}-J_1(\Gamma)e^{-i\omega_m t}]\end{aligned} \tag{2.4}$$

representing the carrier, the upper sideband, and the lower sideband. Here, Γ is the modulation depth, and $J_0(\Gamma)$ and $J_1(\Gamma)$ are Bessel functions of the first kind [Oliver '72]. We ignore the terms in $J_2(\Gamma)$ and above, because the modulation depth for our experiment was small ($\Gamma = 0.49$) and the higher order terms appear at higher harmonics.

There are a series of approximations we can make to the expressions of the output fields of the Michelson interferometer if we consider only the three primary frequencies which emerge from the phase modulator. First, the transmitted port of the Michelson interferometer is actively servoed to the dark fringe of the carrier, so we rewrite the asymmetry length a as

$$a \equiv A + \delta, \tag{2.5}$$

where A is the nominal asymmetry of 8cm and δ is the variation from that asymmetry. Since these variations are quite small, it is reasonable to make the approximations

$$\sin(2k_0 a) = \sin(2k_0 A + 2k_0\delta) \approx 2k_0\delta \quad \text{and} \quad \cos(2k_0 a) = 1 \tag{2.6}$$

where k_0 is the wavenumber of the carrier.

Next we define the wavenumbers for the upper and lower sidebands to be $k_+ \equiv k_0 + k_{SB}$, and $k_- \equiv k_0 - k_{SB}$ where $k_{SB} = \omega_m/c$. We make the approximations

$$\begin{aligned}\sin(2k_+a) &= \sin(2k_0A + 2k_{SB}A + 2k_0\delta + 2k_{SB}\delta)\\ &\approx \sin(2k_0\delta + 2k_{SB}A)\\ &\approx 2k_0\delta\cos(2k_{SB}A) + \sin(2k_{SB}A)\end{aligned} \tag{2.7}$$

and

$$\sin(2k_-a) \approx 2k_0\delta\cos(2k_{SB}A) - \sin(2k_{SB}A) \tag{2.8}$$

$$\cos(2k_+a) \approx \cos(2k_{SB}A) - 2k_0\delta\sin(2k_{SB}A) \tag{2.9}$$

$$\cos(2k_-a) \approx \cos(2k_{SB}A) + 2k_0\delta\sin(2k_{SB}A). \tag{2.10}$$

We make a further approximation to the amplitude of the fields reflected by the Michelson interferometer by adding a loss term, L, which represents the power lost to absorption, scattering, and light conversion into higher order spatial modes. This reflectivity loss reduces the power reflected by the Michelson interferometer by a factor of $1-L$, reducing the reflected field by $\sqrt{1-L}$. The two dominant loss mechanisms in this experiment, at the power levels used, were unwanted reflections from the back surface of the beamsplitter (see section 5.2.1) and the contrast loss caused by thermal lensing of the beamsplitter (see chapter 4).

We include the loss, and rewrite the field reflectivity of the Michelson interferometer for the carrier as

$$\begin{aligned}r_{M0} &= \frac{E_r(k_0)}{E_{in}(k_0)} = \sqrt{1-L}\,e^{-ik_0 2c}\cos(2k_0a)\\ &\approx \left(1-\frac{L}{2}\right)e^{-ik_0 2c}.\end{aligned} \tag{2.11}$$

We combine eqns. 2.2 and 2.9 to get the upper sideband reflectivity,

$$r_{M+} \approx \left(1-\frac{L}{2}\right)e^{-ik_0 2c}e^{-ik_{SB}2c}[\cos(2k_{SB}A) - 2k_0\delta\sin(2k_{SB}A)] \tag{2.12}$$

and likewise combine eqns. 2.2 and 2.10 to get the lower sideband reflectivity.

$$r_{M-} \approx \left(1-\frac{L}{2}\right)e^{-ik_0 2c}e^{ik_{SB}2c}[\cos(2k_{SB}A) + 2k_0\delta\sin(2k_{SB}A)] \tag{2.13}$$

If we assume that the field transmission and reflection of the beamsplitter are reasonably well matched, then the transmission of the Michelson interferometer for the carrier field in the TEM_{00} mode is found by combining eqns. 2.3 and 2.6.

$$t_{M0} \approx ie^{-ik_0 2c} 2k_0\delta \tag{2.14}$$

The transmission for the sidebands is found by combining eqns. 2.3 and 2.7 or 2.8.

$$t_{M+} \approx ie^{-ik_0 2c} e^{-ik_{SB} 2c}(2k_0\delta\cos(2k_{SB}A) + \sin(2k_{SB}A)) \tag{2.15}$$

$$t_{M-} \approx ie^{-ik_0 2c} e^{ik_{SB} 2c}(2k_0\delta\cos(2k_{SB}A) - \sin(2k_{SB}A)) \tag{2.16}$$

Using these expressions for the transmission and reflection coefficients, we can derive the behavior of the recycling cavity.

2.2 Power Recycling Cavity

Since the Michelson interferometer is highly reflective, we can treat it as a mirror with frequency sensitive transmission and reflection described by eqns. 2.11 - 2.16. Instead of throwing the reflected power away, it is stored within an optical resonator called the "power recycling cavity", a Fabry-Perot cavity formed between the Michelson "mirror" and a cavity input mirror, commonly called the recycling mirror.

The field inside a Fabry-Perot cavity like the one shown in figure 2.3 can be easily related to the incident field for slowly varying configurations.

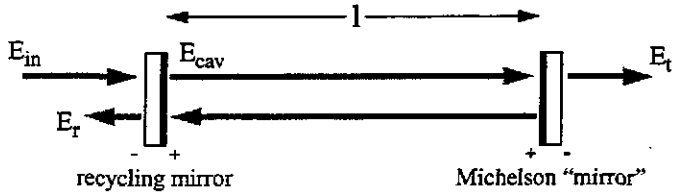

Figure 2.3: Fields within a Fabry-Perot cavity

The steady state field within the cavity is

$$E_{cav}(k) = E_{in}(k)\frac{t_{RM}}{1 - r_{RM} \cdot r_{MM}(k) \cdot e^{-ik2l}} \tag{2.17}$$

where $r_{MM}(k)$ [§] is the field reflectivity of the Michelson "mirror", and t_{RM} and r_{RM} are the field transmission and reflectivity of the recycling mirror. The field transmitted by the recycling cavity is related to the field within the cavity by the transmission of the rear mirror and the extra propagation phase.

§. The Michelson interferometer's asymmetry adds a strong frequency dependence to the reflectivity.

$$E_{out}(k) = E_{cav}(k) \cdot t_{MM}(k) \cdot e^{-ikl} = E_{in}(k) \frac{t_{RM} \cdot t_{MM}(k) \cdot e^{-ikl}}{1 - r_{RM} \cdot r_{MM}(k) \cdot e^{-ik2l}} \qquad (2.18)$$

It is worth considering how the transmission of the recycling cavity is related to the transmission of the rear Michelson "mirror". If $E_{cav}(k)$ were unaffected by differential phase shifts in the Michelson interferometer, then a standard Michelson interferometer with a large input power would be identical to a recycled Michelson interferometer with a proportionately smaller input power (for dynamic cavities, this is only true for measurements at frequencies below pole frequency of the recycling cavity, which is 13kHz for this interferometer). Since the cavity field is a function of the reflectivity of the Michelson interferometer, this comparison does not strictly hold, but two approximations used in the following section do lead to that result. Both approximations hold when the Michelson interferometer's antisymmetric port is near the dark fringe of the carrier. First, the reflectivity for the carrier is proportional to $\cos(2k_0 a)$, which we set to 1 in eqn. 2.6. Second, as is shown in eqn. 2.30, the signal we measure results from the product of the fixed component of the carrier transmission with the fluctuating component of the sideband transmission and from the product of the fixed component of the sideband transmission with the fluctuating component of the carrier transmission. Since the fixed component of the carrier transmission in the TEM_{00} mode is held to 0, the fluctuations in the sideband reflection and transmission are ignored.

Using the expressions for the transmission and reflection coefficients of the Michelson "mirror", we can describe the transmission coefficients of the recycling cavity. Again, several approximations are used. First, the carrier and the sidebands are resonant in the recycling cavity, so

$$e^{-ik_0 2(l+c)} = 1, \qquad e^{-ik_+ 2(l+c)} = 1, \qquad e^{-ik_- 2(l+c)} = 1. \qquad (2.19)$$

The cavity transmission for the carrier becomes

$$t_0 = \frac{E_{out}(k_0)}{E_{in}(k_0)} = \frac{t_{RM} \cdot ie^{-ik_0 2c} 2k_0 \delta \cdot e^{-ikl}}{1 - r_{RM} \cdot \left(1 - \frac{L}{2}\right)}. \qquad (2.20)$$

If we absorb the losses from the recycling mirror into the loss L of the Michelson "mirror," we can rewrite the recycling mirror reflectivity as

$$r_{\mathrm{RM}} = \sqrt{1 - t_{\mathrm{RM}}^2} \approx 1 - \frac{T_{\mathrm{RM}}}{2} \tag{2.21}$$

where $T_{\mathrm{RM}} = t_{\mathrm{RM}}^2$ is the power transmission of the recycling mirror. The carrier transmission then simplifies to

$$t_0 \approx \frac{2it_{\mathrm{RM}} \cdot 2k_0\delta \cdot e^{-ik_0(l+2c)}}{T_{\mathrm{RM}} + L}. \tag{2.22}$$

We now examine the transmission coefficients for the sidebands. By substituting the expressions for the Michelson interferometer interactions with the sidebands (eqns. 2.12 - 2.16) into the cavity output field equation (2.18), we get the sideband transmission of the recycled Michelson interferometer. The transmission for the upper sideband is

$$t_+ \approx \frac{t_{\mathrm{RM}} \cdot ie^{-i(k_0+k_{\mathrm{SB}})(2c+l)}(2k_0\delta\cos(2k_{\mathrm{SB}}A) + \sin(2k_{\mathrm{SB}}A))}{1 - r_{\mathrm{RM}} \cdot \left(1 - \frac{L}{2}\right)(\cos(2k_{\mathrm{SB}}A) - 2k_0\delta\sin(2k_{\mathrm{SB}}A))} \tag{2.23}$$

and the transmission of the lower sideband is

$$t_- \approx \frac{t_{\mathrm{RM}} \cdot ie^{-i(k_0-k_{\mathrm{SB}})(2c+l)}(2k_0\delta\cos(2k_{\mathrm{SB}}A) - \sin(2k_{\mathrm{SB}}A))}{1 - r_{\mathrm{RM}} \cdot \left(1 - \frac{L}{2}\right)(\cos(2k_{\mathrm{SB}}A) + 2k_0\delta\sin(2k_{\mathrm{SB}}A))}. \tag{2.24}$$

For convenience, let $SA \equiv \sin(2k_{\mathrm{SB}}A)$ and $CA \equiv \cos(2k_{\mathrm{SB}}A) \approx 1 - SA^2/2$. We can then rewrite the transmissions as

$$t_+ \approx \frac{2t_{\mathrm{RM}} \cdot ie^{-i(k_0+k_{\mathrm{SB}})(2c+l)}(2k_0\delta\, CA + SA)}{T_{\mathrm{RM}} + L + (SA^2 + 4k_0\delta\, SA)} \tag{2.25}$$

and

$$t_- \approx \frac{2t_{\mathrm{RM}} \cdot ie^{-i(k_0-k_{\mathrm{SB}})(2c+l)}(2k_0\delta\, CA - SA)}{T_{\mathrm{RM}} + L + (SA^2 - 4k_0\delta\, SA)}. \tag{2.26}$$

Using these expressions for the interferometer transmission, we can examine the impact of changing the differential length on the transmitted light power.

We recall that the form of the field incident on the interferometer (eqn. 2.4) is

$$E_{\mathrm{in}} = \sqrt{P_{\mathrm{in}}}(J_0(\Gamma)e^{i\omega t} + J_1(\Gamma)e^{i(\omega+\omega_{\mathrm{m}})t} - J_1(\Gamma)e^{i(\omega-\omega_{\mathrm{m}})t}) \tag{2.27}$$

where P_{in} is the input power, Γ is the modulation index, and $J_0(\Gamma)$ and $J_1(\Gamma)$ are Bessel functions. Let

$$J_0 \equiv J_0(\Gamma) \qquad J_1 \equiv J_1(\Gamma)$$

so the output field is

$$E_{out} = \sqrt{P_{in}} e^{i\omega t}(t_0 J_0 + t_+ J_1 e^{i\omega_m t} - t_- J_1 e^{-i\omega_m t}) \ . \tag{2.28}$$

The output power, $E_{out}{}^* E_{out}$, then has components at DC, the modulation frequency, and twice the modulation frequency. The power at the output of the interferometer at the modulation frequency is

$$P_{mod} = P_{in}[e^{i\omega_m t}(\bar{t}_0 \bar{J}_0 t_+ J_1 - t_0 J_0 \bar{t}_- \bar{J}_1) + e^{-i\omega_m t}(t_0 J_0 \bar{t}_+ \bar{J}_1 - \bar{t}_0 \bar{J}_0 t_- J_1)] \ . \tag{2.29}$$

The signal in this term is used to measure the deviations from the dark fringe. We see that the power at the modulation frequency is the carrier field heterodyned with the sideband fields. The interferometer length is generated by mixing down the power on the photodiode with a reference from the signal used to modulate the light.

To evaluate 2.29, we must expand the products $\bar{t}_0 t_+$, $\bar{t}_0 t_-$, and their conjugates to first order in $k_0\delta$. If we let $\psi \equiv k_{SB}(2c + l)$, then these products become

$$\begin{aligned} \bar{t}_0 t_+ &= \frac{-2it_{RM} \cdot 2k_0\delta \cdot e^{ik_0(l+2c)}}{T_{RM} + L} \cdot \frac{2t_{RM} \cdot ie^{-i(k_0 + k_{SB})(2c+l)}(2k_0\delta\, CA + SA)}{T_{RM} + L + (SA^2 + 4k_0\delta\, SA)} \\ &\approx \frac{8T_{RM} \cdot SA}{(T_{RM} + L) \cdot (T_{RM} + L + SA^2)} \cdot k_0\delta \cdot e^{-i\psi} \end{aligned} \tag{2.30}$$

and

$$\bar{t}_0 t_- \approx \frac{-8T_{RM} \cdot SA}{(T_{RM} + L) \cdot (T_{RM} + L + SA^2)} \cdot k_0\delta \cdot e^{i\psi} . \tag{2.31}$$

We can now write the expression for the output power at the modulation frequency. Since this power is detected by a photodiode, we will also include η, the quantum efficiency of the detector, which is about 0.85 electrons/ photon for our detector [Csatorday '98]. The detected output power at the modulation frequency is